

**Supplemental information****Molecular isoforms of HMGB1 are novel mechanistic biomarkers for epilepsy**

Lauren Elizabeth Walker\*, Federica Frigerio\*, Teresa Ravizza, Emanuele Ricci, Karen Tse, Rosalind E Jenkins, Graeme John Sills, Andrea Jorgensen, Luca Porcu, Thimmasettappa Thippeswamy, Tiina Alapirtti, Jukka Peltola, Martin J Brodie, Brian Kevin Park, Anthony Guy Marson, Daniel James Antoine, Annamaria Vezzani & Munir Pirmohamed.

**Supplemental Table 1**

<i>Exp group</i>	<i>Number of seizure at 2.5 months post-SE</i>	<i>Number of seizure at 4.5 months post-SE</i>	<i>Progression index</i>
Vehicle	9	41	4.56
Vehicle	3	8	2.67
Vehicle	6	8	1.33
Vehicle	3	20	6.67
Vehicle	0	2	n.a.
Vehicle	4	60	15.00
Vehicle	0	3	n.a.
Vehicle	7	3	0.43
Vehicle	2	1	0.50
Treatment	1	2	2.00
Treatment	4	10	2.50
Treatment	2	4	2.00
Treatment	29	75	2.59
Treatment	10	7	0.70
Treatment	11	3	0.27
Treatment	28	1	0.04
Treatment	15	0	0.00
Treatment	0	0	0.00

Number of spontaneous seizures and seizure progression index in vehicle- and drug-treated rats exposed to electrical status epilepticus (SE). n.a.: not applicable refer to rats in which no seizures were detected at 2.5 months. For statistical analysis we attributed to these two rats the average value of progression measured in the corresponding vehicle group. Gray area includes rats which did not progress in each experimental group. All rats were used for statistical analysis.

**Supplemental Table 2.** *Clinical characteristics of patients with drug-resistant epilepsy*

		Epilepsy characteristics					Seizure
Age	Sex	Epilepsy syndrome	Duration (years)	Seizure freq/month	AEDs (Number)	Brain Imaging	Type
36	F	TLE	17	16	2	hippocampal sclerosis	CPS
58	F	TLE	42	17.5	3	hippocampal sclerosis	CPS
33	F	TLE	22	4	2	hippocampal sclerosis, left parietal gliosis, left frontal signal change	CPS
26	M	xTLE	22	14	2	cortical dysplasia in right parietal lobe	CPS
43	M	TLE	2	1	1	normal	SGTCS
22	F	xTLE	3	1	0	normal	SGTCS
52	F	xTLE	52	47.5	3	cortical dysplasia in left frontal lobe and venous anomaly in left parietal lobe	CPS
39	M	TLE	12	15	2	normal	CPS
16	F	xTLE	1	35	4	normal	CPS
26	M	xTLE	9	200	3	vascular lesion in the right temporoparietal lobes	SPS
45	F	IGE	32	1.5	4	vascular lesion left frontotempoparietal lobe	PGS
30	M	TLE	25	2.5	3	hippocampal sclerosis and hamartoma	CPS
41	F	xTLE	31	31	2	normal	CPS
52	M	TLE	52	5	3	hippocampal sclerosis and signal change in left frontal lobe	CPS
31	F	xTLE	31	75	3	normal	CPS
17	F	xTLE	1	12	3	cortical dysplasia in left temporofrontal lobes	CPS
58	F	TLE	32	9.5	3	normal	CPS
22	F	xTLE	17	60	4	cortical dysplasia in right frontal lobe	CPS
28	M	TLE	16	1	2	hippocampal sclerosis	SGTCS
57	F	TLE	56	3	1	hippocampal sclerosis	CPS
20	F	TLE	14	26	3	cortical dysplasia in right and left temporoparietal lobes	SPS
37	M	xTLE	37	6	3	normal	SGTCS
21	M	xTLE	4	22.5	3	signal change in right frontal lobe	CPS
23	M	xTLE	23	30	3	normal	CPS
33	M	xTLE	15	5	1	normal	CPS
32	M	TLE	7	0.5	1	hippocampal sclerosis	CPS
23	F	xTLE		25	1	normal	CPS
45	M	xTLE	5	75	3	signal change in the right gyrus cingulare	SPS

38	M	TLE	4	4	4	gliosis in right temporal lobe	CPS
27	F	IGE	17	0.5	2	normal	PGS
35	M	TLE	35	6	2	normal	CPS
18	F	xTLE	7	15	2	cortical dysplasia in the left frontal lobe	SPS
44	F	TLE	26	0.5	2	hippocampal sclerosis	SGTCS
42	M	TLE	39	10	2	hippocampal sclerosis	CPS
32	M	xTLE	25	60	2	left vascular lesion and bilateral cortical dysplasia	CPS
49	F	xTLE	31	0.5	3	normal	SPS
47	F	xTLE	36	240	2	right cortical dysplasia	CPS
20	F	xTLE	4	0.5	2	normal	CPS
27	F	IGE	18	1.5	1	normal	PGS
39	F	TLE	19	22	2	hippocampal sclerosis	CPS
31	F	xTLE	5	240	3	right slight hemimegalencephalia	CPS
28	F	TLE	24	8	2	hippocampal sclerosis	CPS
47	F	TLE	4.5	3	3	left parietal gliosis after meningeoma operation and left temporo-mesial atrophy	CPS
25	M	xTLE	13	60	3	vascular lesion in right frontotemporal lobe	CPS
25	M	xTLE	13	60	2	normal	CPS
45	M	xTLE	44	70	4	normal	CPS
46	M	TLE	33	5	1	cortical dysplasia in left occipital lobe	CPS
17	M	xTLE	15	28	3	normal	SGTCS
43	M	TLE	24	30	2	cortical dysplasia in left temporal lobe	CPS
27	F	IGE	6	4	1	normal	PGS
31	F	TLE	19	3	2	hippocampal sclerosis	CPS
32	M	TLE	9	4	2	signal change in left amygdala	CPS
27	F	TLE	8	28	3	normal	SGTCS
20	F	IGE	3	4	2	normal	CPS
30	F	TLE	18	2	3	hippocampal sclerosis	CPS
28	F	TLE	2	4	2	normal	SPS
46	M	TLE	25	28	3	normal	SGTCS
26	F	TLE	16	4	4	normal	CPS
53	M	TLE	28	12	3	hippocampal sclerosis	CPS
39	M	IGE	14	6	4	normal	SGTCS
32	M	TLE	9	4	3	hippocampal sclerosis	CPS
65	F	TLE	40	1	2	normal	CPS
31	M	IGE	12	12	3	normal	CPS
60	F	TLE	13	4	4	normal	CPS
23	F	xTLE	14	8	2	normal	SGTCS

22	F	xTLE	22	84	2	normal	SGTCS
46	M	xTLE	8	12	3	left hippocampal atrophy	CPS

M: Male; F: Female;

TLE: Temporal Lobe Epilepsy; xTLE: Extra-temporal lobe epilepsy;

IGE: Idiopathic Generalised Epilepsy;

CPS: Complex Partial Seizure;

SGTCS: Secondarily Generalised Tonic Clonic Seizure;

PGS: Primary Generalised Seizure;

SPS: Simple Partial Seizure;

n/a: information not available

**Supplemental Table 3.** *Clinical characteristics of patients with drug responsive, seizure-free epilepsy*

Age (years)	Sex	Epilepsy Syndrome	Duration (years)	Duration seizure-free (months)	AEDs (number)
26	M	TLE	11	24	1
73	F	IGE	18	24	1
19	M	JME	2	12	1
45	F	TCS	26	11	2
39	F	TLE	2	11	2
19	F	TLE	9	6	2
28	M	xTLE	10	6	1
24	M	IGE	5	14	2
42	F	xTLE	34	13	1
24	F	xTLE	12	20	1
27	M	JA	11	24	1
32	M	IGE	4	6	1
25	F	xTLE	22	24	2
59	M	IGE	2	6	1
21	F	IGE	2	15	2
42	F	TLE	8	10	1
24	F	TLE	11	14	1
22	F	IGE	15	84	1
48	M	xTLE	3	36	1
21	F	IGE	6	18	1

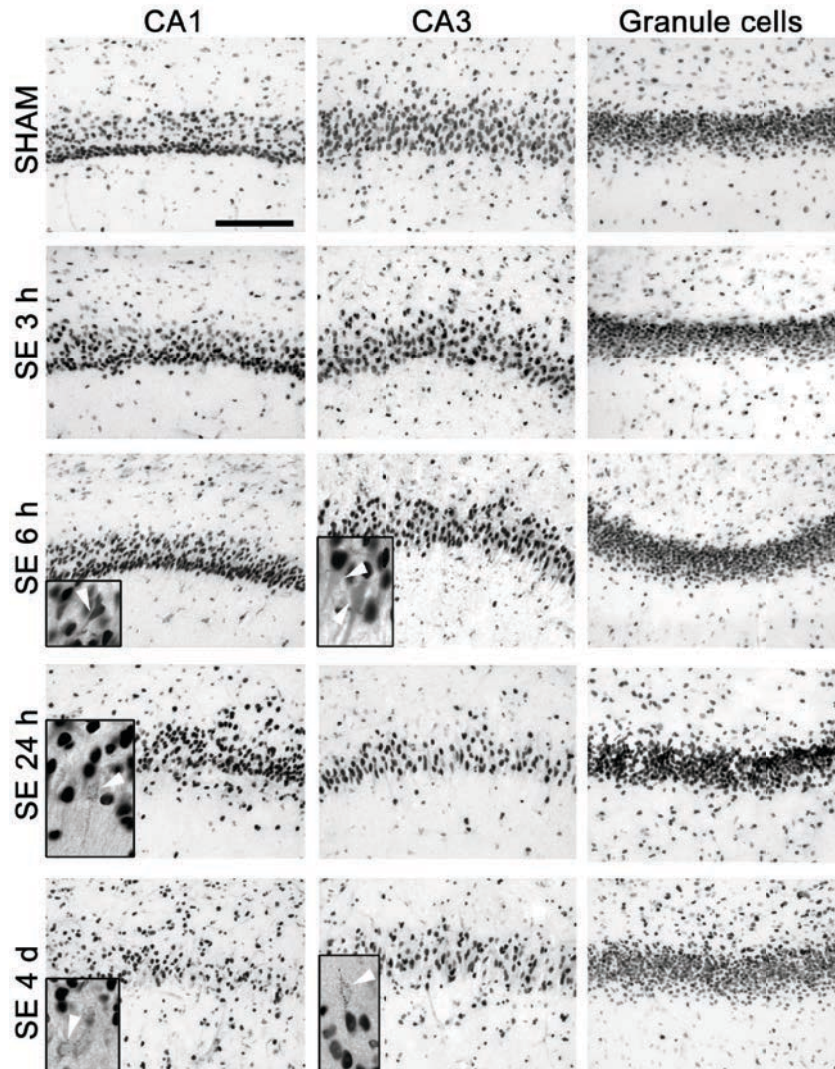
M: Male; F: Female; TLE: Temporal Lobe Epilepsy; IGE: Idiopathic Generalised Epilepsy; JME: Juvenile Myoclonic Epilepsy; xTLE: Extra-temporal lobe epilepsy; JAE: Juvenile Absence Epilepsy

**Supplemental Table 4.** *Comparative characteristics of the patient groups*

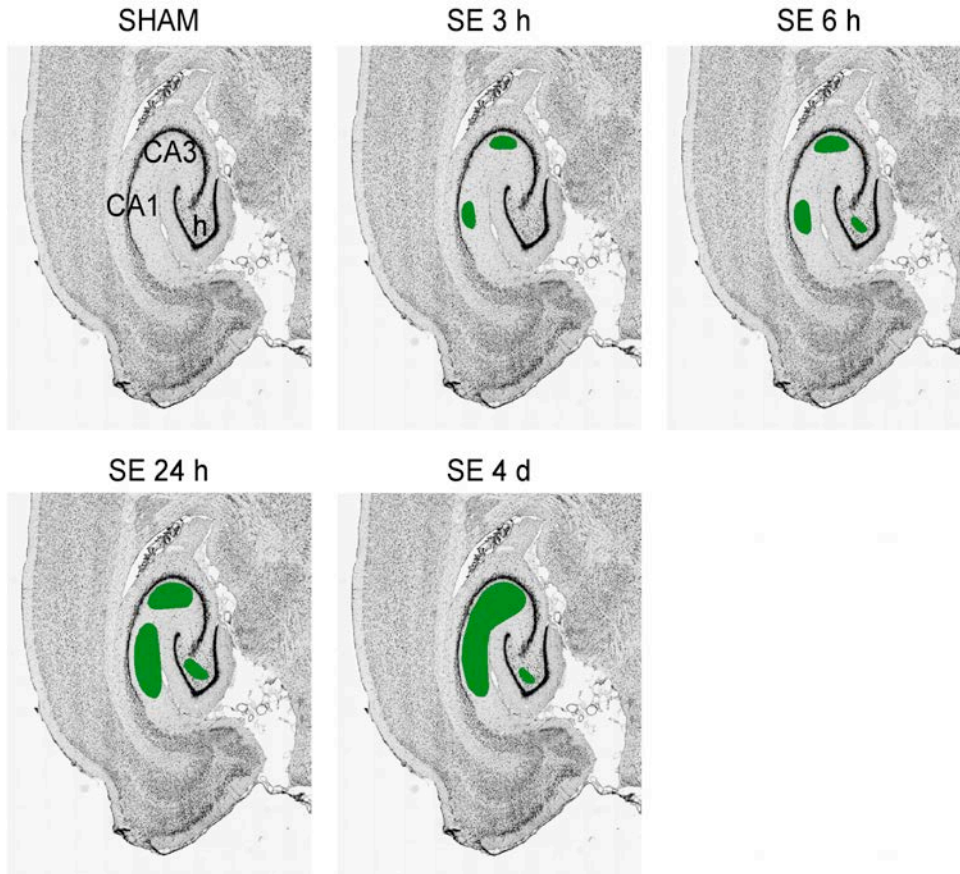
	Healthy controls	Epilepsy Seizure-free (>6m)	Epilepsy Drug-resistant
Number of Patients	74	20	65
Age, years (range)	34 (18-49)	33 (19-73)	34.8 (17-65)
Male/Female	35/37	8/12	28/37
Epilepsy Type (symptomatic/Idiopathic)	n/a	9/11	58/7
Mean duration epilepsy, years (range)	n/a	10.7 (2-34)	19.5 (1-56)
Anti-epileptic therapy: • mono/polytherapy • mono/dual/triple/quad	0	12/8 12/8/0/0	8/57 8/24/25/8
Mean monthly seizure frequency (range)	0	0.004 (0-0.2)	26.8 (0.5-240)
Serum HMGB1 ng/ml, mean $\pm$ s.e.m	1.11 $\pm$ 0.07	1.25 $\pm$ 0.15	8.70 $\pm$ 0.47

HMGB1: High Mobility Group Box-1

## Supplemental Figure 1

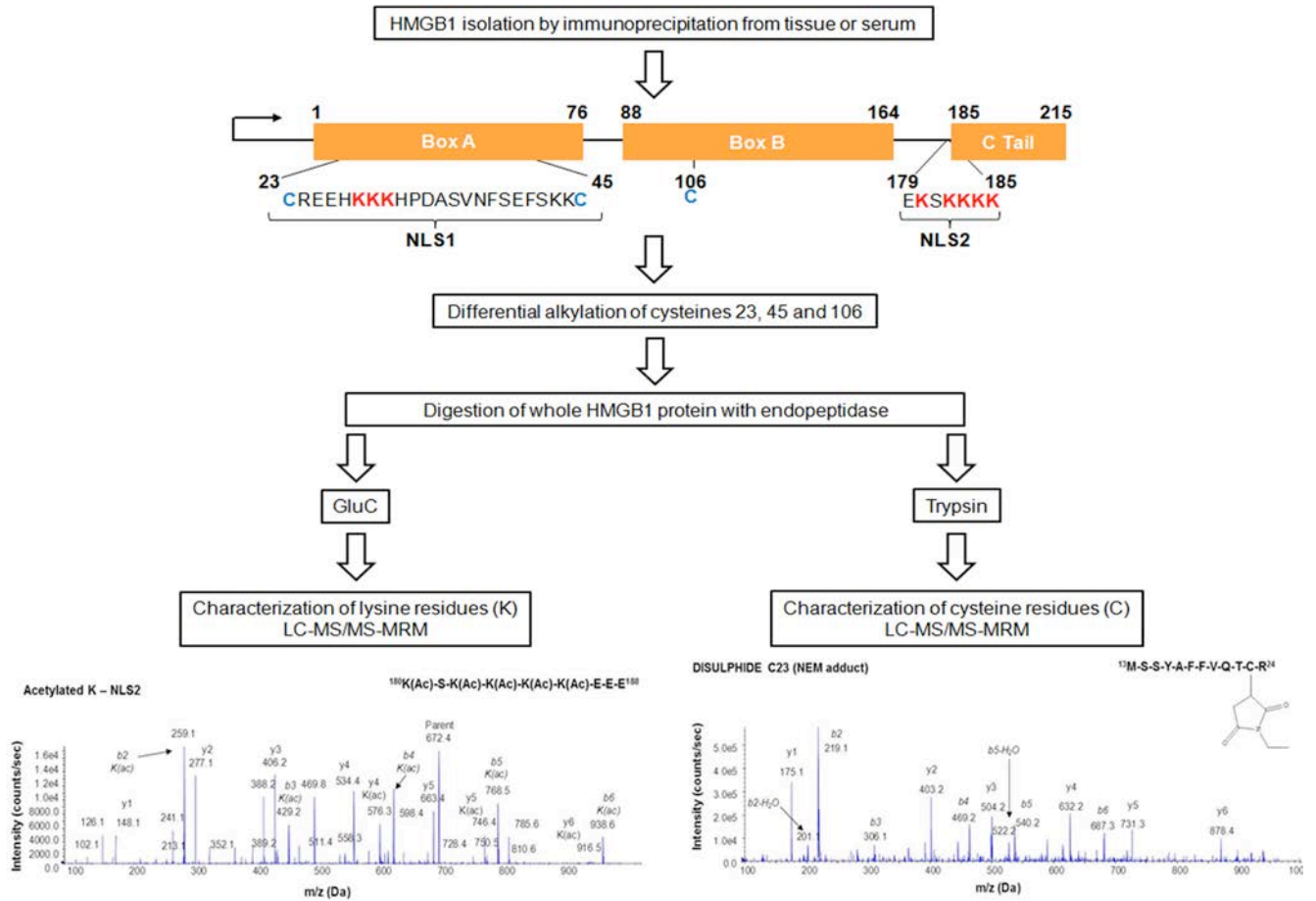


*Neuronal HMGB1 immunoreactivity during epileptogenesis in the hippocampus of electrical status epilepticus (SE) rats.* Immunohistochemical photomicrographs showing HMGB1 staining in CA1 and CA3 pyramidal cell layers and in granule cells of the dentate gyrus in control rats (SHAM), and at representative time points after SE (n=5 each group). Insets depict cytoplasmic HMGB1 staining (white arrowheads) in neuronal clusters as detected in 30% of rats. Brains are from the same rats of the experiment depicted in Figure 1A. Scale bar: 25  $\mu\text{m}$ ; insets 10  $\mu\text{m}$ .

**Supplemental Figure 2**

*Schematic representation of the progressive increase in microglia and astrocytes with cytoplasmic HMGB1 staining (depicted in Figure 1A) in the hippocampus during epileptogenesis evoked by electrical status epilepticus (SE) in rats. CA1, CA3 pyramidal cell layer; h: hilus.*

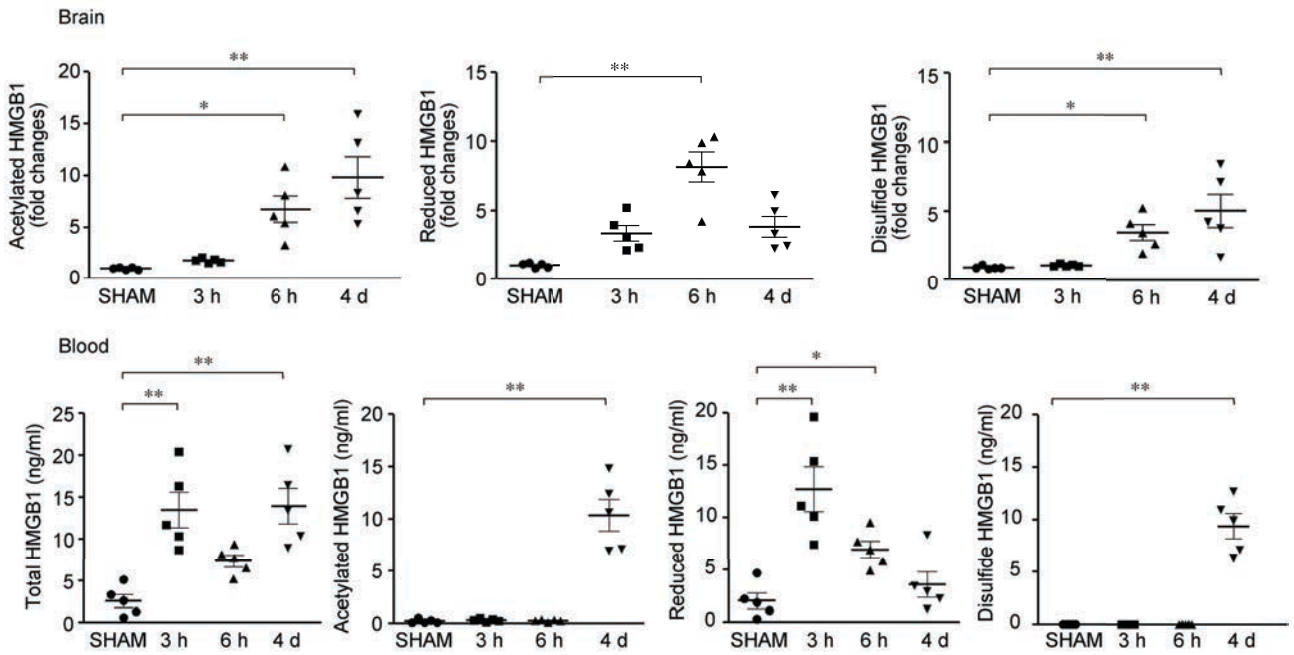
## Supplemental Figure 3



*Schematic overview of the workflow to characterize and quantify post-translational modifications of HMGB1 isoforms isolated from serum and brain tissue.* HMGB1 (representative molecular structure given with labelled amino acids with the one letter code) is isolated by immunoprecipitation and cysteine residues are alkylated by differential alkylation to lock in redox states as previously described (1). Half of the immunoprecipitation of HMGB1 is digested with endopeptidase trypsin. Resulting peptides are characterized by electrospray ionization liquid chromatography tandem mass spectrometry (LC-MS/MS) and quantified by an Multiple Reaction Monitoring (MRM) protocol of an authentic heavy labelled peptide standard. For representation, a HMGB1 derived peptide following trypsin digestion spanning amino acids 13-24 containing cysteine 23 that has been alkylated with N-ethylmaleimide (NEM) is shown (1564.7 Da). Cysteines alkylated with iodoacetamide are characterized as fully reduced and those alkylated with NEM are characterized as participating in a disulfide bond (1). Since proteolytic cleavage by trypsin occurs

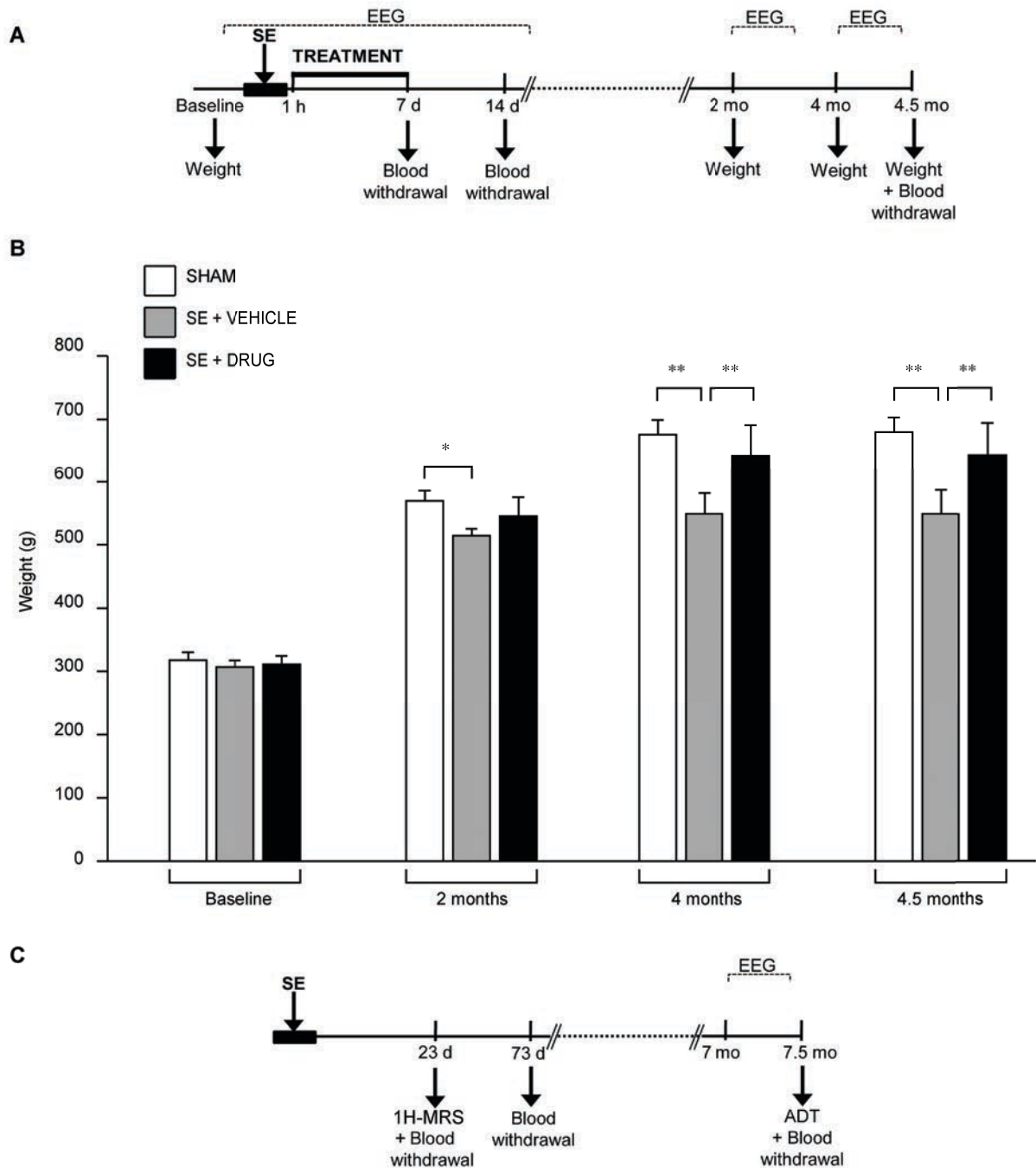
following K residues, GluC digestion must be used to characterize K post translational acetyl-modifications in resulting peptides from the remaining fraction of the immunoprecipitation reaction. Therefore, C redox and K acetyl modifications can not be achieved from the same digestion for HMGB1. A representative peptide sequence spanning K residues within Nuclear Localisation Sequence 2 (NLS2) derived following HMGB1 digestion with GluC is given (1342.6 Da). MS/MS analysis of b and y ions generated from these peptides confirms the amino-acid sequence of each peptide and also the addition of a specific post translational or alkylation modification. On each MS/MS spectra, b and y ions are labelled as required.

## Supplemental Figure 4



Dot plots of individual data related to Figure 1B. Levels of HMGB1 isoforms in brain tissue (hippocampus) and corresponding blood of rats during epileptogenesis. Individual rat values are reported as dot plots (n=5 each group). \*p<0.05, \*\*p<0.01 by Kruskal-Wallis test. Blood acetylated and disulfide HMGB1 levels at 4 days are significantly different from corresponding 3 h and 6 h levels (p<0.01).

## Supplemental Figure 5



Panel (A) depicts the experimental design in adult rats exposed to electrical status epilepticus (SE): the time window of treatment administration post-SE, EEG recordings and blood withdrawal are reported, as well as the time point at which rats were weighted during the experiment. Video-EEG recordings were done continuously from SE induction until the onset of the first two spontaneous seizures (epilepsy diagnosis), and for 2 consecutive weeks (24/7) at 2 and 4 months post-SE. After SE induction, rats were randomized into treatment and vehicle group (n=9 rats each group).

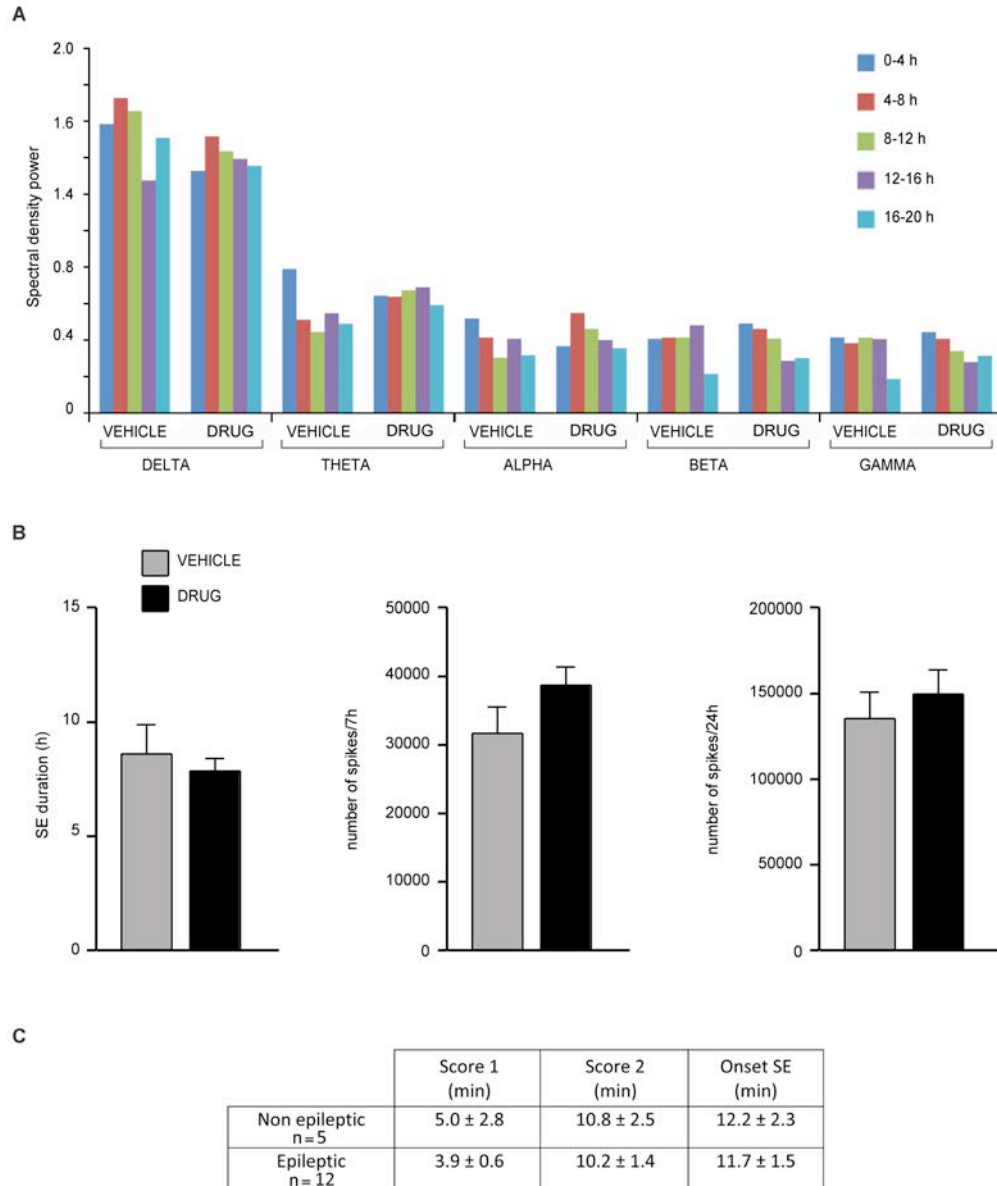
Treatment included anakinra+Box-A+ifenprodil (SE+DRUG) (detailed protocol in Methods). SHAM rats (n= 9) were electrode-implanted but not stimulated, and received vehicles. Data related to this protocol are reported in Figure 2 and Figure 3 in main text, and Suppl. Figures 6A,B and 7-9A.

*Panel (B)*: bargrams reporting the weight of rats at baseline and post-SE during disease development in the vehicle and treatment groups as compared to SHAM rats. \* $p < 0.05$ , \*\* $p < 0.01$  by one-way ANOVA.

*Panel (C)* depicts the time points of blood withdrawal, EEG recording (2 weeks, 24/7) and  $^1\text{H-MRS}$  in P21 rats exposed to SE induced by lithium+pilocarpine. ADT, afterdischarge threshold. Data related to this protocol are reported in Figure 4, Suppl. Figures 10 and 12.

Rats were killed at the end of the last EEG recording session for histological analysis of cell loss.

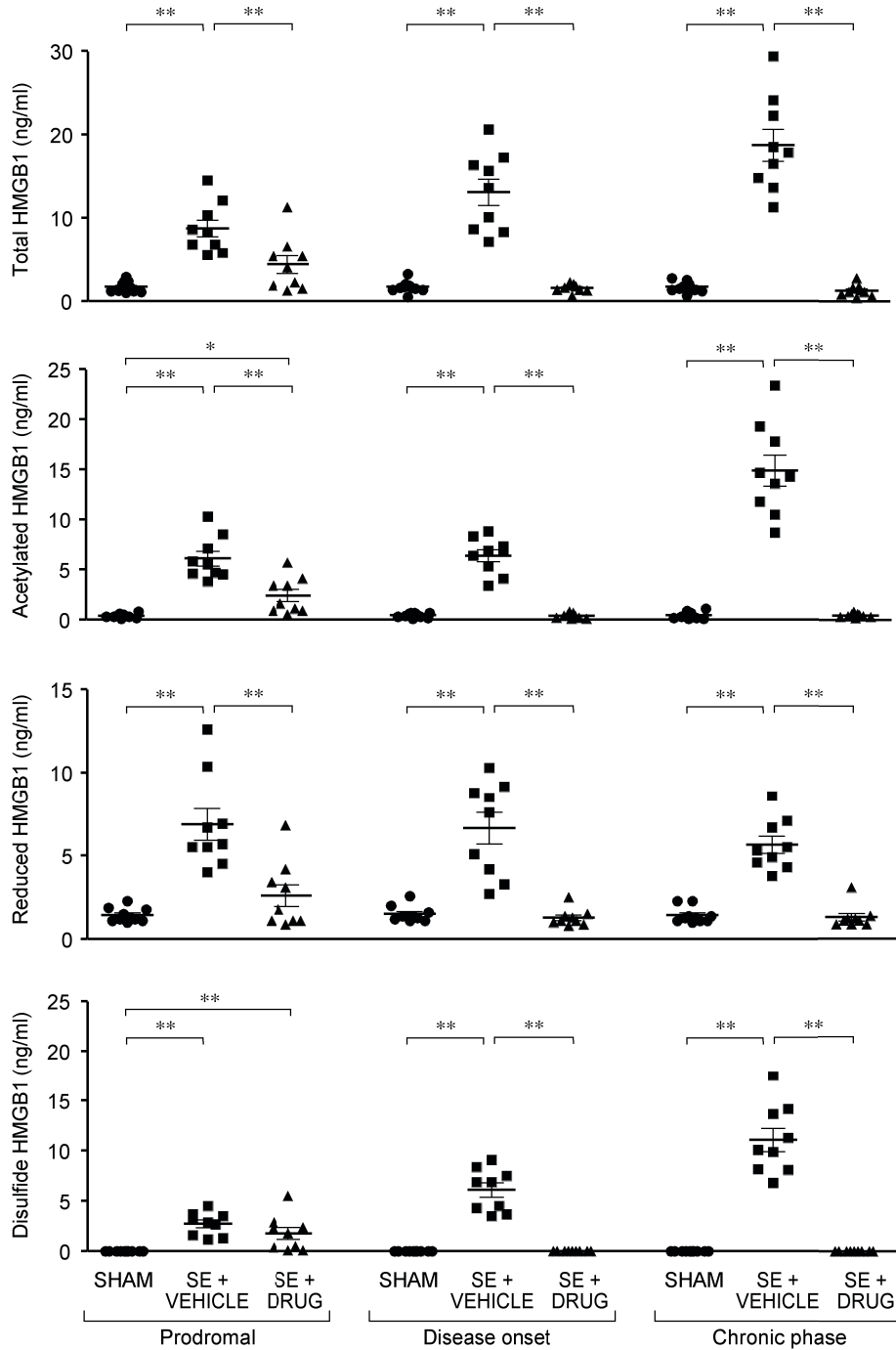
## Supplemental Figure 6



*Quantification measures of status epilepticus (SE) in rats.*

*Panel (A):* EEG spectral analysis of electrical SE in adult rats receiving vehicle or anti-inflammatory drugs (n=9 each group). *Panel (B):* Quantitative measures of SE as assessed by EEG analysis. Rats are those depicted in main text Figures 2 and 3 and in Suppl. Figure 7. *Panel (C):* Behavioral analysis of SE in P21 rats exposed to lithium+pilocarpine (n=17). Epileptic (n=12) and non epileptic (n=5) rats were prospectively identified by EEG analysis of spontaneous seizures and after-discharge threshold at 7.5 months post-SE (see Methods and Results for details). Score 1 and 2 are described in Methods. Rats are those depicted in Figure 4 and Suppl. Figure 10.

## Supplemental Figure 7



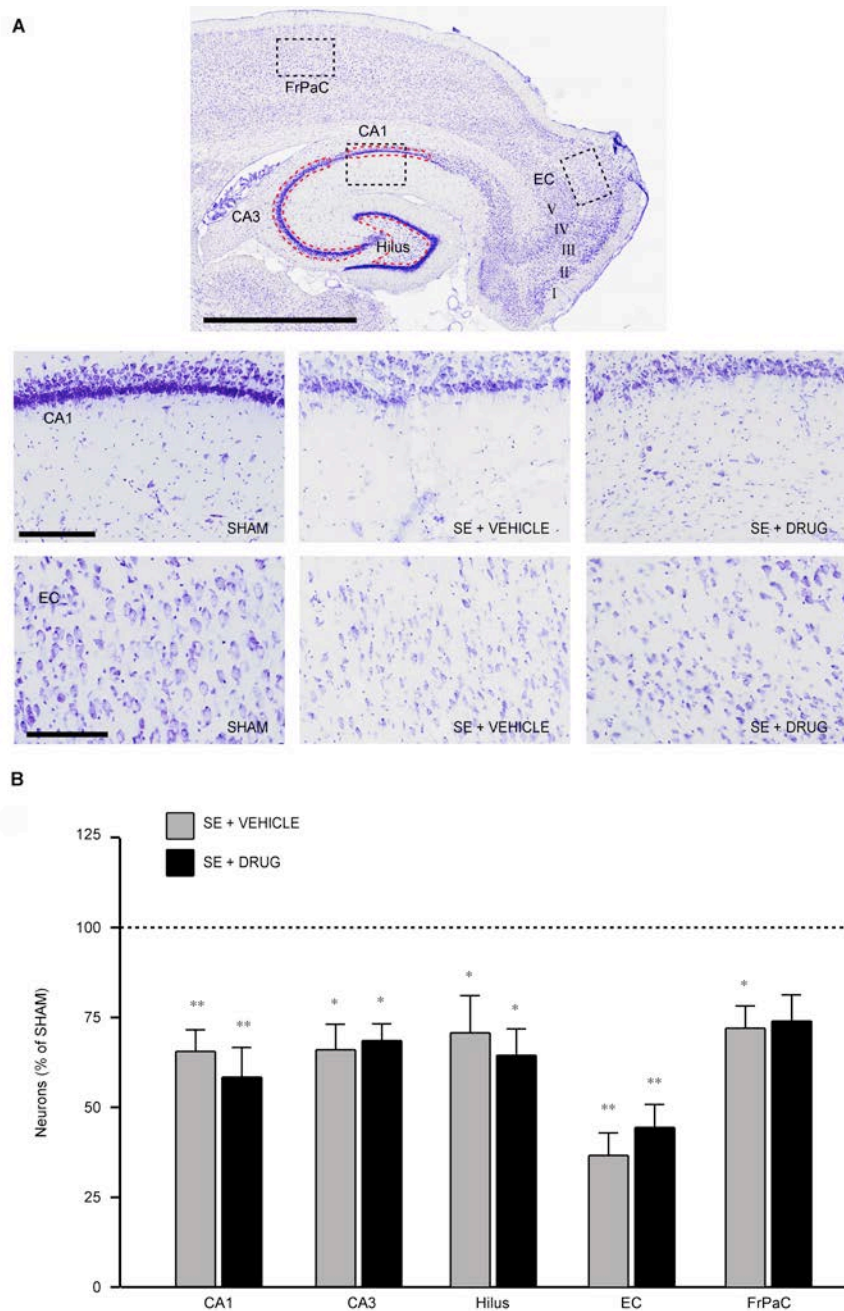
Dot plots of individual data related to Figure 2. Longitudinal analysis of total HMGB1 and levels of acetylated, reduced and disulfide isoforms in blood serum at representative time points of disease development in SE-exposed rats receiving treatment (DRUG) or corresponding VEHICLE. Treatment included anakinra+BoxA+ifenprodil (SE+DRUG) (detailed protocol in Methods; Suppl.

Figure 5A).

Individual rat values are reported as dot plots (n=9 rats each group). \*\*p<0.01 by one-way ANOVA.

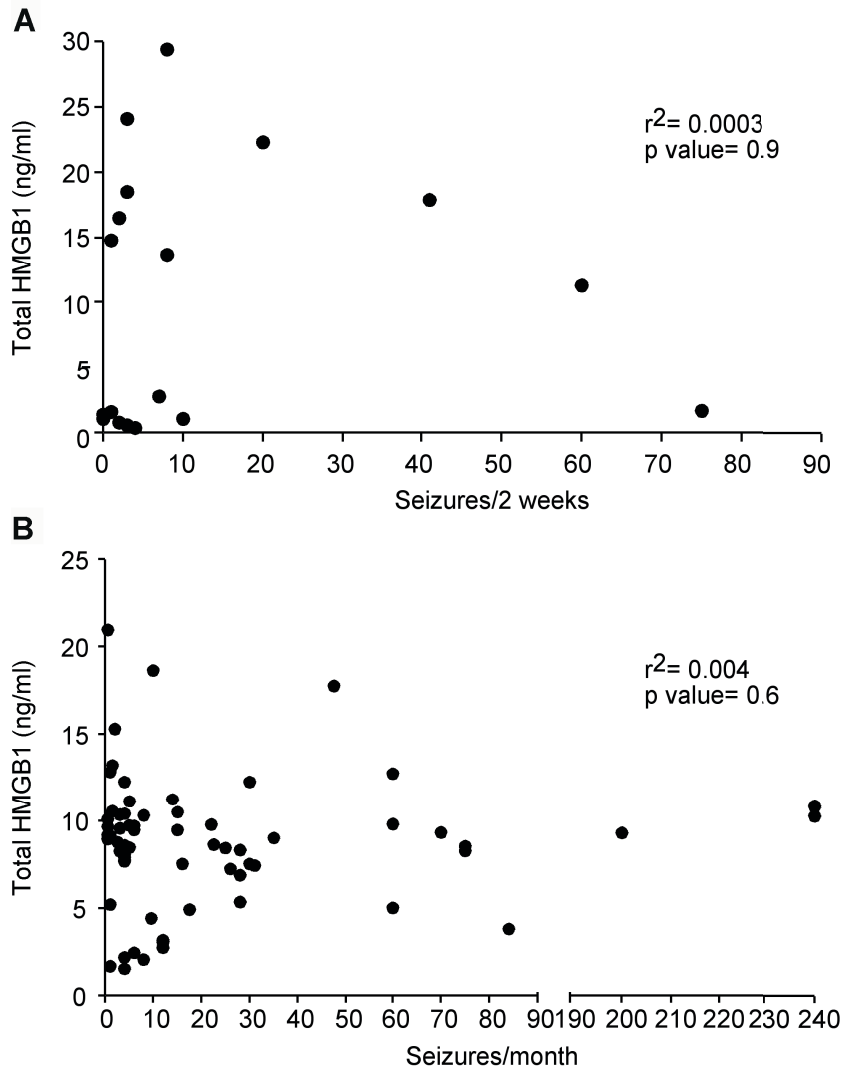
The acetylated isoform level in the chronic phase (SE+VEHICLE) was significantly different from corresponding level at disease onset and prodromal phases (p<0.01 by repeated measures one-way ANOVA). The disulfide isoform (SE+VEHICLE) level at disease onset and in the chronic phase was significantly different from corresponding level in prodromal phase (p<0.05 and p<0.01, respectively); the disulfide isoform level in the chronic phase was significantly different from corresponding level at disease onset (p<0.05 by repeated measures one-way ANOVA).

## Supplemental Figure 8



*Panel (A)* shows representative photomicrographs of Nissl-stained hippocampal sections. *First row*, boxed and dotted areas in the hippocampal slice represent where cell quantification was done. *Panel (B)* shows the relative quantification of neuronal cell loss in rats exposed to electrical SE and treated with vehicle or anti-inflammatory drugs for 1 week (n=9 each group). Rats were killed 4.5 months post-SE (protocol in Suppl. Figure 5A). The lack of neuroprotection differs from findings in Noe' et al (2) which may be due to the lack of administration of VX-765 which inhibits IL-1 $\beta$  biosynthesis. Rats are the same depicted in Figures 2 and 3 and Suppl. Figure 7. *Scale bar*: 250  $\mu$ m; 50  $\mu$ m.

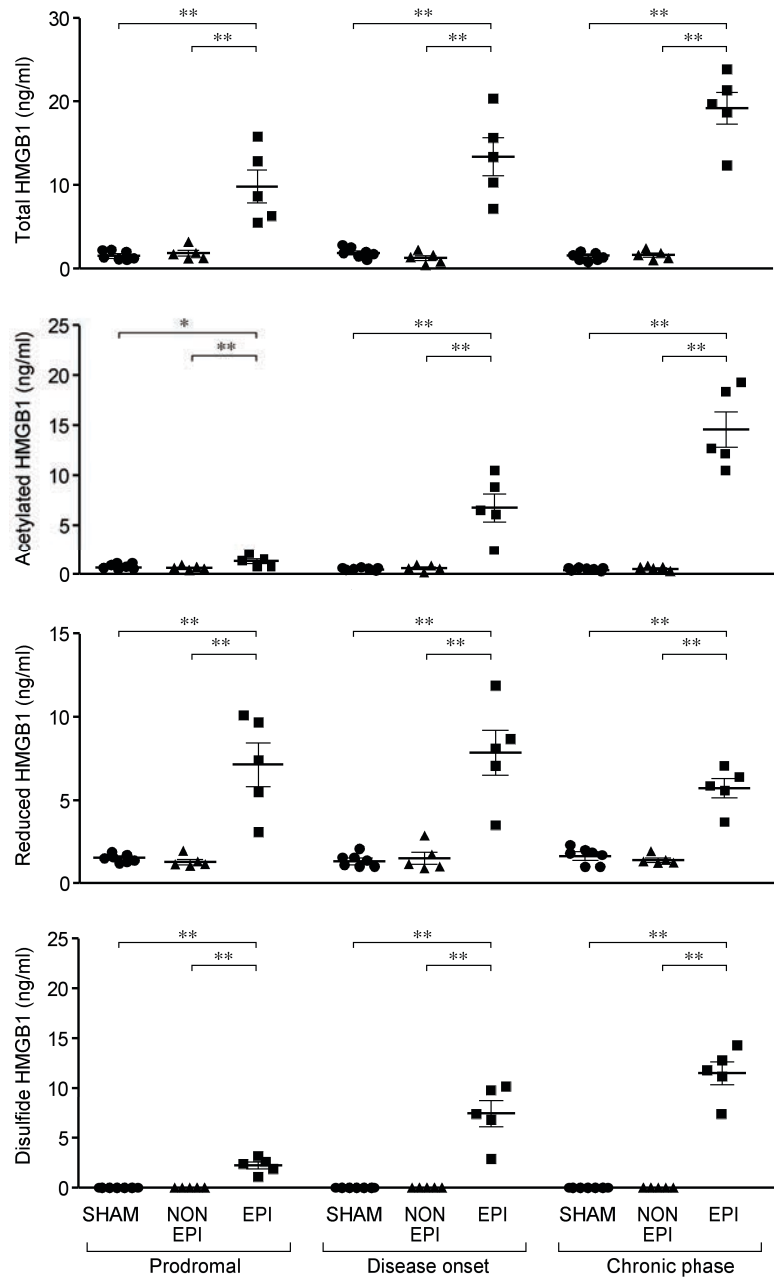
## Supplemental Figure 9



*Panel (A):* Lack of correlation between seizure counts in rats with chronic epilepsy as assessed during 2-week video-EEG recording 4.0-4.5 months post-SE and the relative HMGB1 blood levels collected 4.5 months post-SE (total n=18: vehicle, n=9 and drug-treated, n=9). These are the same rats as in Figure 2 and Figure 3.

*Panel (B):* Lack of correlation between pre-enrolment seizure count (last month before blood withdrawal) and total HMGB1 blood level in patients with drug-resistant epilepsy, i.e., the same patients as in Fig. 5A (n=65).

## Supplemental Figure 10



Dot plots of individual data related to Figure 4. Longitudinal analysis of total HMGB1 and acetylated, reduced and disulfide isoforms level in blood at representative time points of disease development. Blood was drawn at 23 days (*epileptogenic phase* prodromal to epilepsy onset), 73 days (encompassing the *time of disease onset* in 70% of rats) and 7.5 months (chronic epilepsy). Individual rat values are reported as dot plots (n=7 SHAM; n=5 EPILEPTIC, EPI; n=5 NON EPILEPTIC, NON EPI) rats. \*\*p<0.01 by Kruskal-Wallis test. Total HMGB1, acetylated and

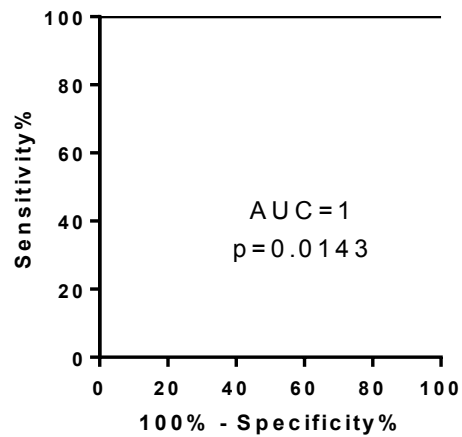
disulfide isoform levels in the chronic phase (EPI) are significantly different vs corresponding levels in prodromal phase ( $p < 0.01$  by repeated measures one-way ANOVA).

## Supplemental Figure 11

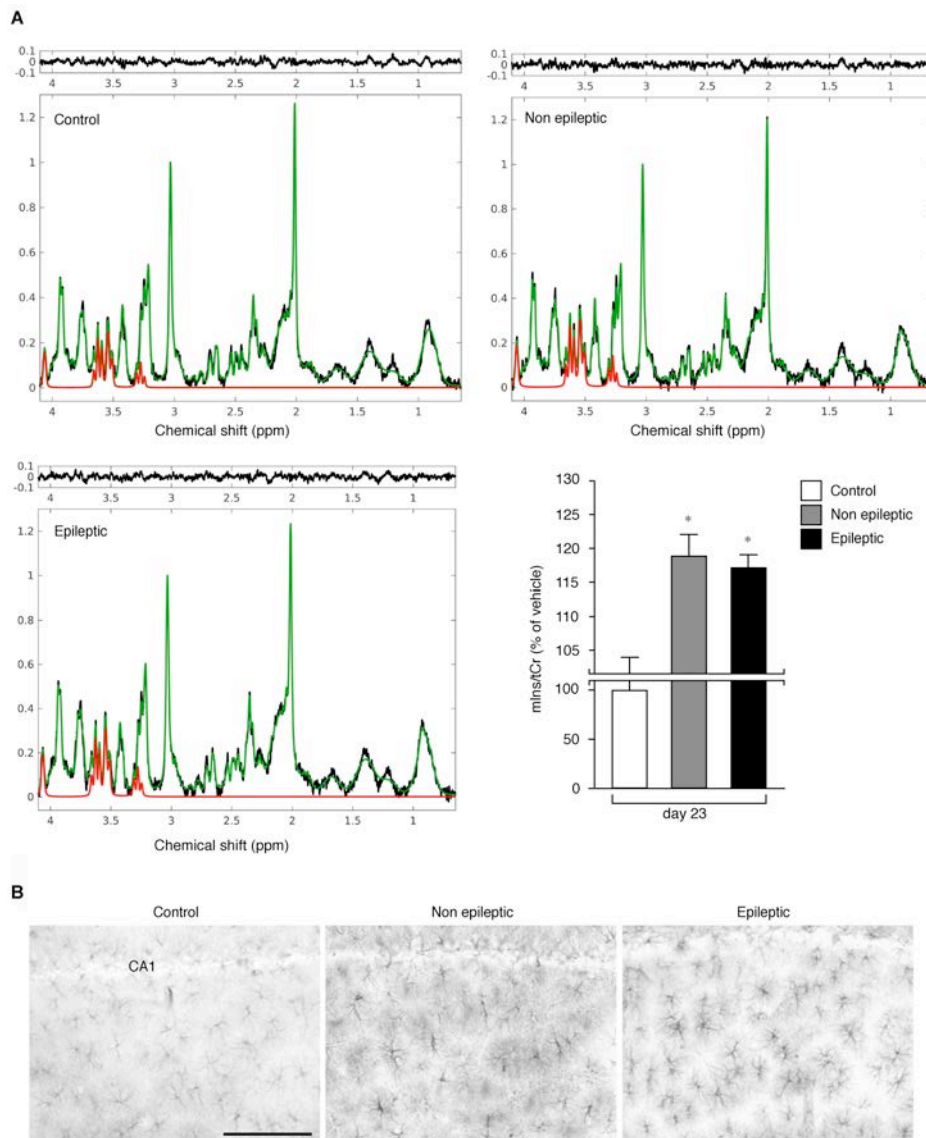
*Example of ROC analysis related to Fig. 4A*

Prodromal phase – Epileptic vs Non epileptic rats (Total HMGB1)

Cut off	Sensitivity%	95% CI	Specificity%	95% CI
< 1.25	25	0.6309% to 80.59%	100	47.82% to 100%
< 1.5	50	6.759% to 93.24%	100	47.82% to 100%
< 2.45	75	19.41% to 99.37%	100	47.82% to 100%
< 4.35	100	39.76% to 100%	100	47.82% to 100%
< 5.9	100	39.76% to 100%	80	28.36% to 99.49%
< 7.5	100	39.76% to 100%	60	14.66% to 94.73%
< 10.8	100	39.76% to 100%	40	5.274% to 85.34%
< 14.35	100	39.76% to 100%	20	0.5051% to 71.64%



## Supplemental Figure 12



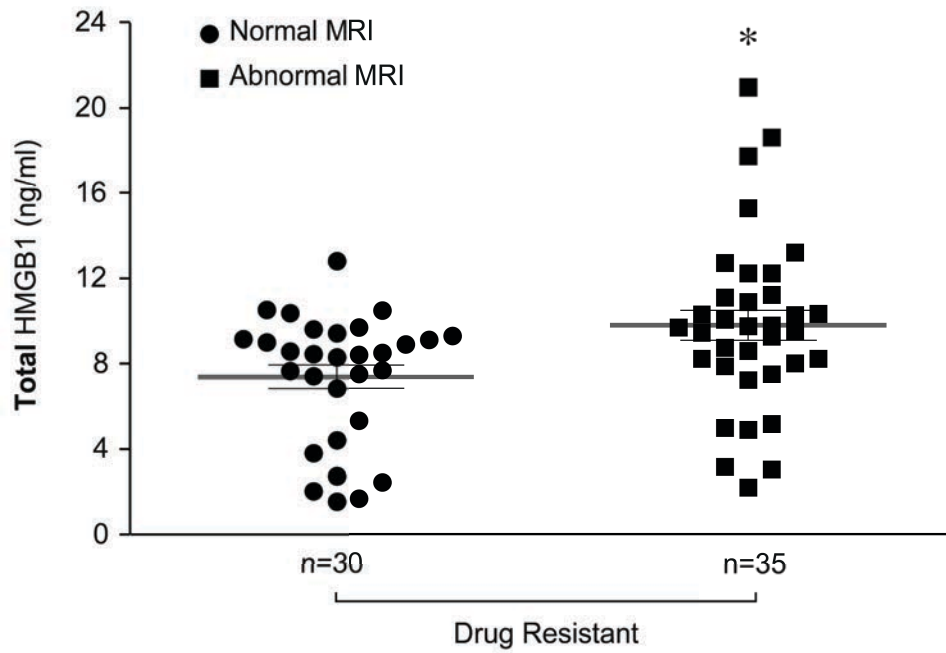
*Panel A:  $^1\text{H}$ -MRS analysis of mIns/tCr levels in the hippocampus during epileptogenesis.* Representative  $^1\text{H}$ -MRS spectra acquired at day 23 post-SE (prodromal phase) in rats which did not develop epilepsy at 7.5 months post-SE (non epileptic,  $n=5$ ) and epileptic rats ( $n=5$ ) developing epilepsy at 7.5 months post-SE. Control rats ( $n=7$ ) were age-matched sham-implanted and vehicle-injected animals not exposed to SE. These animals are the same as reported in Figure 4B from which the corresponding blood was withdrawn at the time of imaging, i.e., during the prodromal phase (*protocol in Suppl. Figure 5C*). Spectra and fit residuals (*upper row*) are plotted in black, metabolite fits are plotted in green, and mIns contribution, a metabolite reflecting astrocyte activation (3), is plotted in red. Bargram depicts the mIns/tCr levels (mean  $\pm$  s.e.m.) in the various

experimental groups. mIns/tCr levels were increased at the same extent in epileptic and non epileptic rats compared to controls therefore showing a similar astrocytic activation state. \* $p < 0.05$  vs control by one-way ANOVA followed by Kruskal-Wallis's test.

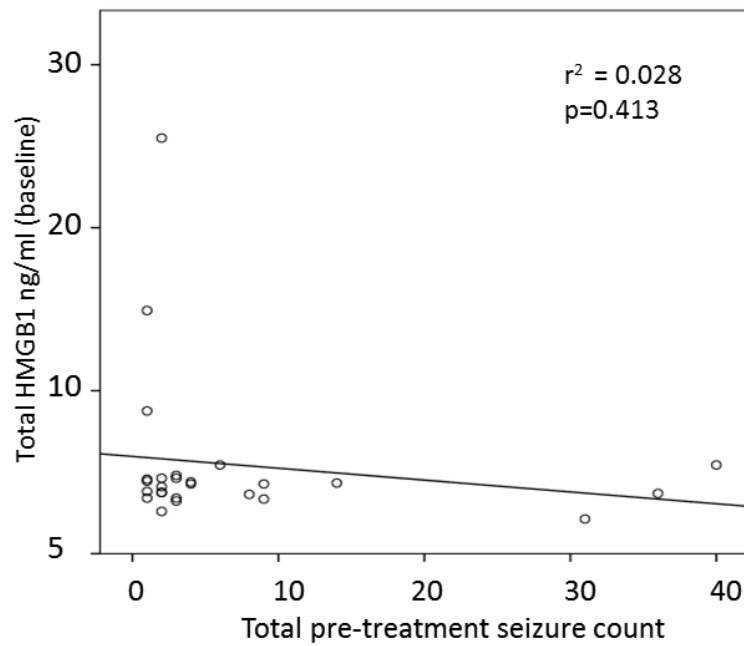
*Panel (B): GFAP expression in the hippocampus of rats with and without spontaneous seizures as assessed by video-EEG analysis 7 months post-SE.* Representative photomicrographs showing GFAP-immunoreactive astrocytes in the CA1 region. Epileptic and non epileptic rats (same rats as in *panel A*) show similar GFAP immunostaining in activated astrocytes exhibiting hypertrophic cell body, long and thick processes. Control rats show GFAP immunoreactivity in stellate-shaped astrocytes with thin processes denoting their resting state. *Scal bar: 50  $\mu$ m.*

<sup>1</sup>H-MRS analysis and spectra quantification have been performed as previously described in detail (4,5) on a 7T Bruker Biospin 70/30 Avance III system, equipped with a 12 cm diameter gradient coil (400 mT/m maximum amplitude). Briefly, a PRESS (Point Resolved Spectroscopy) sequence (repetition time TR/TE = 2500/10 ms, 512 scans, spectral width 20 ppm, 8192 points) was carried out in a single voxel (14  $\mu$ L) positioned randomly in the septal left or right pole of the hippocampus. Water suppression was performed with VAPOR and first and second order shims were adjusted using FASTMAP (Fast, Automatic Shimming technique by Mapping Along Projections). <sup>1</sup>H-MRS spectra were quantified using TARQUIN 4.2.1 (6) for the estimation of mIns levels. Each spectrum was pre-processed by applying automated zero-order phasing and referencing, and by performing residual water line removal with the HSVD method. The processed signal was fit to a linear combination of selected metabolites. The reliability and quality of the fitting procedure was assessed both by visual inspection and by checking the quality parameter Q retrieved by TARQUIN. The mean value of Q was included between 1.15 and 1.3, indicating a very high fit quality (Q= 1 corresponds to a perfect fit) (6). The amplitudes of the mIns signals obtained by the fit that had a CRLB (Cramer-Rao lower bound) higher than 35% were excluded from the results (none of the rats was excluded). Relative mIns levels were then derived by scaling the fitted amplitudes by the amplitude of the total Creatine (tCr: Cr + phospho Cr) signal, considered as the internal standard.

## Supplemental Figure 13

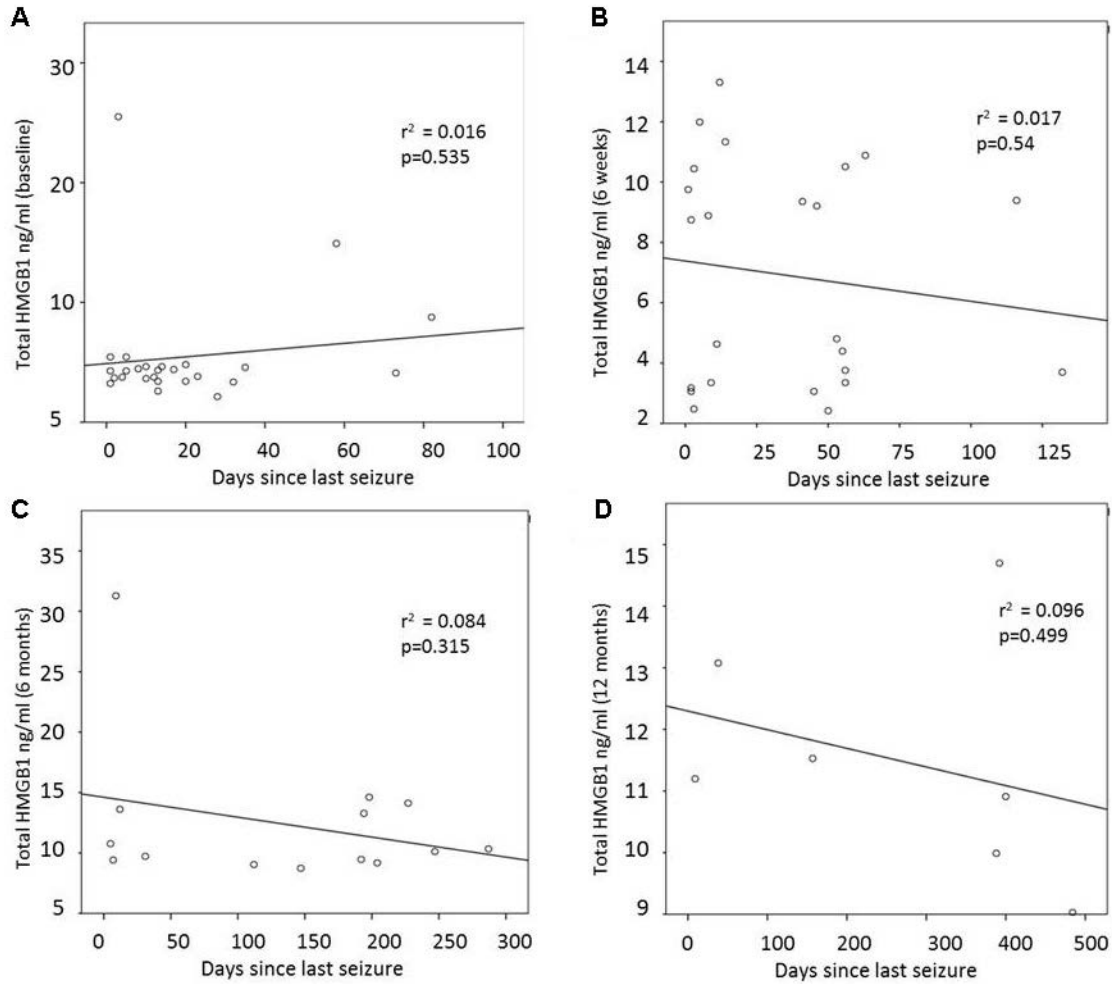


Total HMGB1 levels in blood serum of drug-resistant epilepsy patients (mean  $\pm$  SEM, n=65) with (n=35) or without (n=30) MRI abnormalities. \*p < 0.01 by t-test.

**Supplemental Figure 14**

Lack of correlation between total high mobility group box-1 (HMGB1) and the total pre-treatment seizure count reckoned at diagnosis (baseline visit, n=26) in patients with newly diagnosed epilepsy.

## Supplemental Figure 15



Lack of correlation between total high mobility group box-1 (HMGB1) and the number of days since last seizure in patients with newly diagnosed epilepsy at baseline visit (*panel A*,  $n=26$ ) and 6-weeks (*panel B*,  $n=24$ ), 6-months (*panel C*,  $n=14$ ) and 12-months (*panel D*,  $n=7$ ) following diagnosis.

**Reference list**

1. Yang H, et al. Redox modification of cysteine residues regulates the cytokine activity of high mobility group box-1 (HMGB1). *Mol Med*. 2012;18:250-259.
2. Noé FM, et al. Pharmacological blockade of IL-1beta/IL-1 receptor type 1 axis during epileptogenesis provides neuroprotection in two rat models of temporal lobe epilepsy. *Neurobiol Dis*. 2013;59:183-193.
3. Brand A, Richter-Landsberg C, Leibfritz D. Multinuclear NMR studies on the energy metabolism of glial and neuronal cells. *Dev Neurosci*. 1993;15(3-5):289-298.
4. Pascente R, et al. Cognitive deficits and brain myo-Inositol are early biomarkers of epileptogenesis in a rat model of epilepsy. *Neurobiol Dis*. 2016;93:146-155.
5. Filibian M, Frasca A, Maggioni D, Micotti E, Vezzani A, Ravizza T. In vivo imaging of glia activation using <sup>1</sup>H-magnetic resonance spectroscopy to detect putative biomarkers of tissue epileptogenicity. *Epilepsia*. 2012;53(11):1907-1916.
6. Wilson M, Reynolds G, Kauppinen RA, Arvanitis TN, Peet AC. A constrained least-squares approach to the automated quantitation of in vivo (<sup>1</sup>H) magnetic resonance spectroscopy data. *Magn Reson Med*. 2011;65(1):1-12.

## **Supplemental Methods**

### **Molecular isoforms of HMGB1 are novel mechanistic biomarkers for epilepsy**

Lauren Elizabeth Walker\*, Federica Frigerio\*, Teresa Ravizza, Emanuele Ricci, Karen Tse, Rosalind E Jenkins, Graeme John Sills, Andrea Jorgensen, Luca Porcu, Thimmasettappa Thippeswamy, Tiina Alapirtti, Jukka Peltola, Martin J Brodie, Brian Kevin Park, Anthony Guy Marson, Daniel James Antoine, Annamaria Vezzani & Munir Pirmohamed.

*Brain preparation for immunohistochemistry and analysis of cell loss*

Rats were deeply anaesthetized using ketamine (150 mg/kg; Alcyon, Italy) and medetomidine (2,0 mg/kg, Alcyon) then perfused with 4% paraformaldehyde in PBS *via* the ascending aorta (1–3). The brains were post-fixed for 90 min at 4 °C, transferred to 20% sucrose in PBS for 24 h at 4 °C, frozen in n-pentane for 3 min at –50 °C, then stored at –80 °C until assayed. Serial horizontal sections (40 µm) were cut on a cryostat throughout the temporal extension of the hippocampus (7.6 to 4.6 mm from bregma) (4). We prepared 7 series of 10 sections each. In each series, the 1<sup>st</sup> and 5<sup>th</sup> sections were stained for Nissl to assess neuronal cell loss. In the 2<sup>nd</sup> and 5<sup>th</sup> series, the 2<sup>th</sup> section was stained for HMGB1. HMGB1 immunostaining was carried out as previously described (5). Briefly, slices were incubated at 4°C for 1 h in 10% fetal bovine serum (FBS) in 0.1% Triton X-100 in PBS, followed by an overnight incubation with the primary antibody against HMGB1 (ab18256; 1:1000; Abcam, Cambridge, UK; 1DegreeBio for validation information) at 4°C in 10% FBS in 0.1% Triton X-100 in PBS. Immunostaining was absent when slices were incubated with the primary antibodies preabsorbed with the corresponding peptides, or without the primary antibodies (5). Two rats for each time point were randomly chosen for triple immunostaining to identify the cells expressing HMGB1. Two brain slices adjacent to those used for HMGB1 immunohistochemistry were used for each cell type marker. After incubation with the primary HMGB1 antibody, slices were incubated with an anti-rabbit biotinylated secondary antibody (BA-1000; 1:200, Vector Labs, Burlingame, CA, USA), then in streptavidin–HRP and the signal was revealed with tyramide conjugated to Fluorescein using TSA amplification kit (SAT-701001EA; NEN Life Science Products, Boston, MA, USA). Sections were subsequently incubated with the following primary antibodies: mouse anti-GFAP (MAB3402; 1:3500, Merck Millipore, Livingston, UK) a marker of astrocytes, or mouse anti-OX-42 (MCA275G; 1:1000, Serotec, Oxford, UK), a marker of microglia, or with mouse anti-rat endothelial protein (SMI-71R; EBA, 1:10,000, Sternberger, Lutherville, MD, USA) to identify microvessels. Fluorescence was detected using anti-mouse secondary antibody conjugated with

Alexa546 (A-11030; 1:500; Molecular Probes, Leiden, The Netherlands). Additional incubation in Hoechst 33258 (H3569; 1:500; Molecular Probes) in PBS was done to visualize the cell nucleus. Slide-mounted sections were examined with an Olympus Fluorview laser scanning confocal microscope (microscope BX61 and confocal system FV500) using excitations of 488 nm (Ar laser), 546 nm (He-Ne green laser) and 350 nm (ultraviolet) for fluorescein, Alexa546 and Hoechst, respectively. The emission of fluorescent probes was collected on separate detectors. To eliminate the possibility of bleed-through between channels, the sections were scanned in a sequential mode.

*Assessment of cell loss.* Cell loss was measured in rats at the end of experiments, as previously described (6–8). Briefly, images of the dorsal (P21 model) or temporal (electrical SE model) pole of the hippocampus in each hemisphere were captured at 20X magnification using a BX61 microscope equipped with motorized platform (Olympus, Germany) and digitized. Quantification was done in 4 Nissl-stained coronal sections for each rat brain. Neuronal cell loss in the hippocampus was quantified by reckoning the number of Nissl-stained neurons in CA1 and CA3 pyramidal cell layers and the hilar interneurons. The number of neurons in entorhinal and frontoparietal cortices, was reckoned only in the temporal pole slices (electrical SE model) in two different fields covering cortical layer III in each hemisphere (274 x 165  $\mu\text{m}$  for entorhinal cortex and 414 x 176  $\mu\text{m}$  for frontoparietal cortex) captured at 20X and 10X magnification, respectively. Nissl-positive cells were marked by one investigator blinded to the identity of the samples, and an automated cell count was generated using Fiji software. Data obtained in each section/area/rat were averaged, thus providing a single value for each area per rat, and this value was used for the statistical analysis. Samples underwent the same methodological procedures in parallel by an experienced investigator blinded to the treatment.

**Reference list**

1. Marcon J, et al. Age-dependent vascular changes induced by status epilepticus in rat forebrain: implications for epileptogenesis. *Neurobiol Dis.* 2009;34(1):121-132.
2. Roch C, Leroy C, Nehlig A, Namer IJ. Predictive value of cortical injury for the development of temporal lobe epilepsy in 21-day-old rats: an MRI approach using the lithium-pilocarpine model. *Epilepsia.* 2002;43(10):1129-1136.
3. Ravizza T, Gagliardi B, Noé F, Boer K, Aronica E, Vezzani A. Innate and adaptive immunity during epileptogenesis and spontaneous seizures: evidence from experimental models and human temporal lobe epilepsy. *Neurobiol Dis.* 2008;29(1):142-160.
4. Paxinos G, Watson C. *The Rat Brain in Stereotaxic Coordinates.* New York: Academic Press; 2005.
5. Maroso M, et al. Toll-like receptor 4 and high-mobility group box-1 are involved in ictogenesis and can be targeted to reduce seizures. *Nat Med.* 2010;16(4):413-419.
6. Noé FM, et al. Pharmacological blockade of IL-1beta/IL-1 receptor type 1 axis during epileptogenesis provides neuroprotection in two rat models of temporal lobe epilepsy. *Neurobiol Dis.* 2013;59:183-193.
7. Pascente R, et al. Cognitive deficits and brain myo-Inositol are early biomarkers of epileptogenesis in a rat model of epilepsy. *Neurobiol Dis.* 2016;93:146-155.
8. Filibian M, Frasca A, Maggioni D, Micotti E, Vezzani A, Ravizza T. In vivo imaging of glia activation using <sup>1</sup>H-magnetic resonance spectroscopy to detect putative biomarkers of tissue epileptogenicity. *Epilepsia.* 2012;53(11):1907-1916.